15 Feb 2017

Characterization and Fracture Property of Different Strontium-Containing Borate-Based Glass Coatings for Ti6Al4V Substrates

Yiming Li

Ali Matinmanesh

Declan J. Curran

Emil H. Schemitsch

et. al. For a complete list of authors, see https://scholarsmine.mst.edu/che_bioeng_facwork/1103

Recommended Citation

CrossMark

Characterization and fracture property of different strontium-containing borate-based glass coatings for Ti6Al4V substrates

Yiming Li [a,b], Ali Matinmanesh [a,b], Declan J. Curran [a,b], Emil H. Schemitsch [b], Paul Zalzal [c], Marcello Papini [a], Anthony W. Wren [d], Mark R. Towler [a,b,*]

[a] Mechanical & Industrial Engineering, Ryerson University, Toronto, ON, Canada
[b] Keenan Research Centre, St. Michael's Hospital, Toronto, ON, Canada
[c] Oakville Memorial Hospital, Oakville, ON, Canada
[d] Inamori School of Engineering, Alfred University, Alfred, NY, USA

ABSTRACT

This work considered the effect of increasing Strontium ion (Sr^{2+}) content on the structure of a series of glasses based on the B_2O_3-P_2O_5-$CaCO_3$-Na_2CO_3-TiO_2-$SrCO_3$ series and their resultant fracture toughness when coated onto a surgical metal substrate. Six glasses with increasing Sr^{2+} content (0 to 25 mol%) were synthesized and subsequently characterized by X-ray Diffraction (XRD), Differential Thermal Analysis (DTA) and both Magic Angle Spinning Nuclear Magnetic Resonance (MAS-NMR) and Raman Spectroscopy. These techniques confirmed that increased Sr^{2+} content induced more non-bridging oxygens (NBOs) into the glass network. This would be expected to lead to de-polymerization of the glass structure, as would be evinced by lower glass transition temperatures (T_gs) as Sr^{2+} increased within the glass series. However, T_g was found to increase with Sr^{2+} addition, inferring that the strength of the ionic bond between strontium and oxygen (Sr—O) enhanced network rigidity. The glasses were coated onto Ti6Al4V substrates using an enamelling technique, and the critical strain energy release rates (G_{IC}) of the resultant coating/substrate constructs were measured. The incorporation of 15–25 mol% Sr^{2+} into the glass network was found to significantly increased the toughness of the glass/Ti6Al4V constructs.

© 2016 Elsevier B.V. All rights reserved.

1. Introduction

Scaffolds with structures designed to mimic trabecular bone have been fabricated from borate-based glass precursors using the Robocasting technique [1]. Such glasses can be designed to degrade *in vivo* to induce Hydroxyapatite (HA) formation when in contact with physiological fluids, thereby providing a favorable substrate for the attachment and proliferation of osteogenic cells [2–7], which can assist in the healing of critical-size segmental defects [8]. Borate-based glasses can also facilitate treatment of osteomyelitis by stimulating bone regeneration [9,10].

Borate glass chemistry can be influenced by the addition of different alkali metal and alkaline earth ions thus allowing for tunable solubility and bioactivity [11], through a phenomena known as 'boron anomaly' [12]. Pure vitreous boron oxide (B_2O_3) is primarily constructed of boroxol rings ($[BØ_3]$) (Ø = bridging oxygen) linked together through oxygen atoms [13]. Small amounts (<30 mol%) of alkali oxides (R_2O) and alkaline earth oxides (RO) introduce additional oxygen ions, which convert two $[BØ_3]$ units into two $[BØ_4]$ units. Higher glass network modifier contents (>30 mol%) induce the formation of NBOs on borate triangular units and $[BØ_4]$ tetrahedra. The transformation of $[BØ_3]$ to $[BØ_4]$ induces a fourth bridging boron oxygen bond per boron center, resulting in both an increase in hardness of the glass and a rise in glass transition temperature (T_g), thus reducing the likelihood of the glass degrading in an aqueous environment. However, increased formation of NBOs leads to de-polymerization of the glass network, which decreases T_g [11].

Previous studies [14,15] have considered borate-based glasses for clinical coating applications, confirmed their adhesion to Ti6Al4V-alloys. One of the advantages of borate-based glasses is that, unlike HA and silicate glasses, they can be tailored to have similar coefficients of thermal expansion (CTE) to Ti6Al4V [16], thus minimizing the chances of fracture while cooling when using the glass as a coat [17].

Sr^{2+} incorporation into bioactive glasses increases their hardness [18] and can stimulate bone formation [19] by increasing osteoblastic activity and decreasing osteoclastic activity [20]. The enhanced bioactivity as a result of Sr^{2+} release can also contribute to the formation of a

* Corresponding author at: Department of Mechanical & Industrial Engineering, Faculty of Engineering and Architectural Science, 350 Victoria Street, Toronto, ON M5B 2K3, Canada.
E-mail address: mtowler@ryerson.ca (M.R. Towler).

Table 1
Compositions of the borate based glass series, displayed in mol%.

	LY-B0	LY-B1	LY-B2	LY-B3	LY-B4	LY-B5
B_2O_3	59	54	49	44	39	34
$CaCO_3$	13	13	13	13	13	13
P_2O_5	3	3	3	3	3	3
Na_2CO_3	15	15	15	15	15	15
TiO_2	10	10	10	10	10	10
$SrCO_3$	0	5	10	15	20	25
Total	100	100	100	100	100	100

stable bond between bone and a surgical implant [21]. Therefore, Sr^{2+} incorporation is expected to have a positive influence on the bioactive and mechanical properties of the glass series.

Plasma spraying and enamelling are two common techniques used for coating onto Ti6Al4V substrates. However, the thermal procedure may also cause changes in the microstructure of the coating and substrate materials [22,23]. In addition, the plasma sprayed technique is sometimes limited by the stresses generated during the different stages of the deposition process [24]. Enamelling can be performed under controlled atmospheres and temperatures without inducing structural changes to either the coatings or substrates [25]. The thickness of the coat is also a primary factor influencing adhesion [26,27]. A previous study of silicate glass coatings bonded to Ti6Al4V indicated that the fracture toughness of the systems utilizing ~90 μm thick coatings were higher than that of the systems utilizing thicker coatings (200–400 μm) [28].

Usually, tensile (pull-out) and scratch tests are used to measure adhesion between the coating and substrate [14,29]. However, such techniques only describe adhesion in qualitative terms, and thus cannot be reliably used for comparative purposes between glass systems. In order to quantify the adhesion between the coating and substrate, the Vickers indentation fracture (VIF) test [30] and the interface indentation fracture (IIF) test [31] have been considered. However, these techniques are prone to large errors due to violations of model assumptions during practical testing scenarios [28]. Another quantitative fracture mechanics-based method involves determining the critical mode I strain energy release rate (G_{IC}) using bi-layer double cantilever beam specimens originally developed for study of environmentally degraded structural adhesive joints [32]. Such specimens have recently been demonstrated to yield reliable measures of the G_{IC} for glass coatings bonded to Ti6Al4V-alloys [28].

In this study, a series of borate-based glasses were fabricated with increasing Sr^{2+} loadings (up to 25 mol%) and subsequently characterized by a range of techniques to investigate the influence of increasing Sr^{2+} doping on chemistry of the glass series. The glasses were then coated onto the surface of a Ti6Al4V substrate using an enamelling technique. The influence of different Sr^{2+} incorporations on the G_{IC} of the glass coating/Ti6Al4V substrate systems were then determined using bi-layer double cantilever beam specimens.

2. Materials and methods

2.1. Glass synthesis

Six glasses (Ly-B0 to Ly-B5) were formulated based on the B_2O_3-P_2O_5-$CaCO_3$-Na_2CO_3-TiO_2-$SrCO_3$ glass series with increasing amounts of $SrCO_3$ (from 0 to 25 mol%) at the expense of B_2O_3. The control glass, Ly-B0, was free of $SrCO_3$. The compositions of the glasses are presented in Table 1. Glasses were prepared by weighing out appropriate amounts of analytical grade reagents in powder form, firing the mixtures (1300 °C, 1 h) in a silica crucible, and subsequently shock quenching into water. The resulting frits were dried, ground and sieved to retrieve powders with a mean particle size of <20 μm.

2.2. XRD analysis

Diffraction patterns were collected using a D2 PHASER (Bruker AXS Inc., WI, USA). Powdered samples and coated Ti6Al4V bars were packed into stainless steel sample holders. A generator voltage of 30 kV and a tube current of 10 mA were employed and diffractograms were collected in the range of $20° < 2θ < 80°$, at a scan step size 0.02° and a count time of 0.3 s.

2.3. Particle size analysis (PSA)

PSA was performed using a Beckman Coulter Multisizer 4 Particle size analyzer (Beckman-Coulter, Fullerton, CA, USA). Glass samples were evaluated in the range of 0.4–100.0 μm and the run length was 60s. Characterization was performed in water at room temperature. Three measurements were recorded for each glass composition and the mean and SD were collected for each.

2.4. DTA measurement

A combined differential thermal analyzer-thermal gravimetric analyzer (DTA-TGA, SDT Q600, TA Instruments) was used to measure the T_gs and T_{c1}s for all glass samples. A heating rate of 20 °C/min was employed in a nitrogen (N_2) atmosphere between 0 °C to 1000 °C using $α$-A_2O_3 as a reference.

2.5. MAS-NMR measurement

The ^{31}P and ^{11}B MAS-NMR spectra for the glass series were recorded with a solid echo sequence on a Bruker AVANCE 500 NMR spectrometer (Agilent Technologies, Inc., Santa Clara, CA, USA) using a 2.5 mm MAS probe with spinning speeds of 20 kHz. The 90 degree pulse for the central transition was 1.5 μs. The echo delay was 100 s. Spectra were recorded with at least 32 scans using a 30 s recycle time.
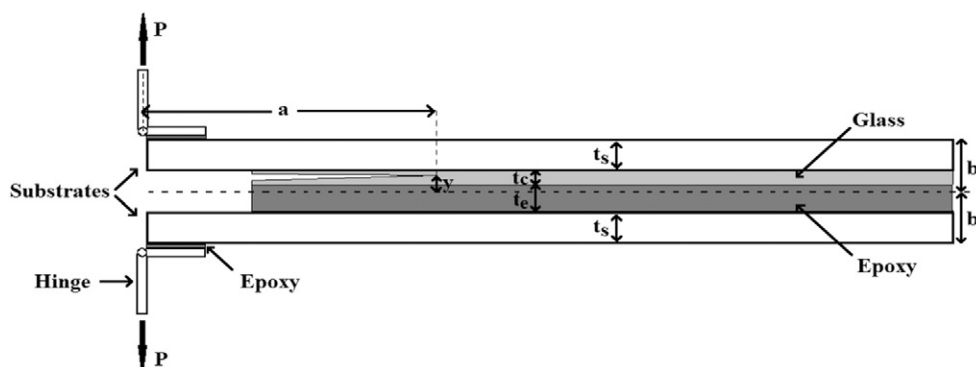

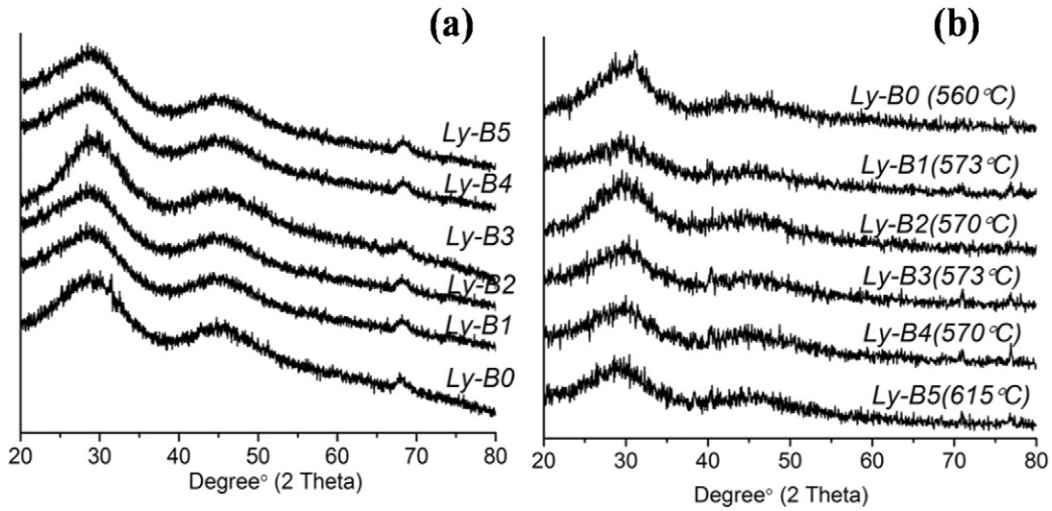**Fig. 1.** Double layer DCB specimen [28].

Fig. 2. The XRD patterns of (a) the original glasses and (b) glass coatings on the Ti6Al4V substrates.

2.6. Raman spectroscopy measurement

Raman analysis was conducted using a Sierra Reader (Snowy Range Instruments, WY, USA), employing a red laser with an excitation wavelength of 785 nm and power of 72 mW. Each scan lasted 10 s and 5 scans in total were performed for each sample, the average of which was recorded. The Sierra Reader built-in software (Snowy Range Peak Software v3.13) combined with GRAMS software (Waltham, MA, USA) was used to generate the spectral data. The peaks in the Raman spectra were fitted using the Gaussian function.

2.7. Fabrication of glass coatings on Ti6Al4V substrate

Ti6Al4V plates (88.9 mm × 12.7 mm × 3.2 mm) (McMaster-Carr, Elmhurst, Illinois, USA) were polished using 1200 grit sand paper and cleaned using ethanol. The average roughness, R_a, of the plates after polishing was found to be 0.5–0.6 μm. In order to release the residual stresses in the Ti6Al4V plates before coating they were heated without any constraints up to 650 °C for 15 min. The furnace was then shut off and the plates were allowed to cool down to the room temperature within the furnace.

Glass powder (<20 μm) and ethanol (0.16 g glass per 1.2 ml ethanol) were mixed inside a standard 5 ml syringe for approximately 1 min and deposited on the surface of the Ti6Al4V plate placed on a leveled table. The coated samples were air-dried for 30 min at room temperature, and then were reheated to a temperature between T_g and T_{c1} for 15 min to keep the glassy nature of the coatings. The furnace was then shut off and the coated samples were allowed to cool down within the furnace.

Coating thicknesses were determined using an optical non-contact profilometer (Microphotonics Inc., NanoveaST400). Three parallel profile traces 4 mm apart along the longitudinal axis of the substrate with a step size of 5 μm were obtained both before and after coating the surface. The waviness profile was extracted by applying a Gaussian filter with a cut-off wavelength of 0.25 mm. The difference in the resulting profiles yielded three thickness profiles per specimen. Point by point averages and standard deviations for each thickness profile were calculated and averaged to obtain the overall average thickness and standard deviation for each specimen.

2.8. Bi-layer DCB specimen

Similar to Matinmanesh et al. [28], bi-layer DCB specimens (Fig. 1) were used to measure the G_{IC}. First, a thin layer of a room temperature

cure epoxy (J-B Weld 8265-S Cold Weld Compound, Sulphur Springs, TX, USA) was spread onto the glass-coated adherents. A 0.7 mm diameter wire was then inserted around the periphery of the coated specimen to ensure that the bond line between glass and the substrate remained visible during the test. The wire was removed after approximately 10 min, by which point the epoxy had set. Then the "double sandwich" specimen was clamped and left at room temperature for 48 h to allow complete cure of the epoxy. Two hinges were glued to the free ends of the specimen (Fig. 1) using the quick set epoxy. The bond line between the glass and substrate was covered with diluted type writer correction fluid, and the length of bond line was marked at fixed intervals to facilitate crack length measurement during testing.

2.9. Measurement of critical strain energy release rate (G_{IC}) of the coating/substrate system

A United Universal Tester (STM series, United Testing Systems, Inc., Huntington Beach, CA, USA) with a 500 N load cell was utilized in displacement control at a crosshead displacement rate of 0.5 mm/min to load the hinges on the specimens using friction grips. The crack propagation was monitored by a digital microscope camera (OptixCam Summit SK2-14X, Roanoke, VA, USA) having a field of view of 3 mm, which was mounted on a motorized stage. As discussed in detail in Matinmanesh et al. [28], multiple G_{IC} measurements could be obtained for each specimen by repeatedly loading the specimen until the crack
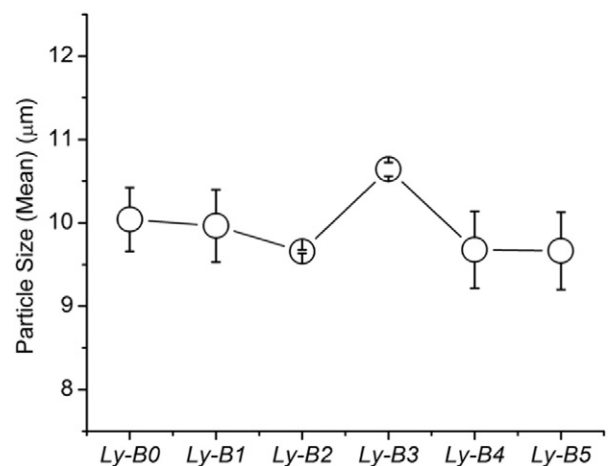

Fig. 3. Particle size of the borate-based glasses.

Table 2
Thermal profiles (DTA curve) of the borate based glass series.

(°C)	Ly-B0	Ly-B1	Ly-B2	Ly-B3	Ly-B4	Ly-B5
T_g	500	510	521	525	535	550
T_{c1}	677	690	650	618	629	649

propagated in a stable manner. Three samples for each coating were tested.

The G_{IC} was calculated as:

$$G_{IC} = \frac{12 P_{\max}^2 a^2}{E_s w^2 t_s^3} \qquad (1)$$

where $P_{\max}$ was the load necessary to propagate the crack, w the width of the substrate, E_s the Young's modulus of the substrate (110 GPa) and a the distance from crack tip to the hinge's axis of rotation (Fig. 1).

2.10. Statistical analysis

One-way analysis of variance (ANOVA) was employed to assess the significance of the changes in the measured G_{IC} and glass particle size brought about by changes in the glass compositions. The comparison of relevant means was performed using the *post hoc* Bonferroni test. Differences between groups were deemed significant when $p \leq 0.05$.

3. Results and discussion

3.1. XRD and PSA

The XRD patterns of the glasses in their as fired forms and as enamelled coatings on the substrates are shown in Fig. 2 (a) and (b), respectively. The broad XRD curves without any detectable sharp peaks confirmed the amorphous nature of all original glasses and coatings. Crystalline phases influence the solubility, biocompatibility and mechanical properties of bioactive glasses [33]. The PSA data of the glass series is shown in Fig. 3. The mean particle size of each glass was approximately 10 μm throughout the series. There was no significant difference ($p \geq 0.05$) between the particle sizes of the six glasses.

3.2. DTA

T_gs and T_{c1}s of the glass series are recorded in Table 2. Fig. 4 shows the variation of glass transition temperature (T_g) of the borate based glass series. T_g can elucidate changes in glass structure resulting from the addition of cations. In this glass series, Sr^{2+} is expected to act as a
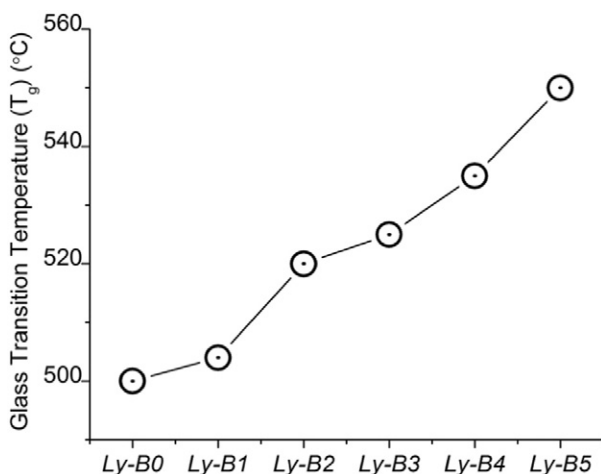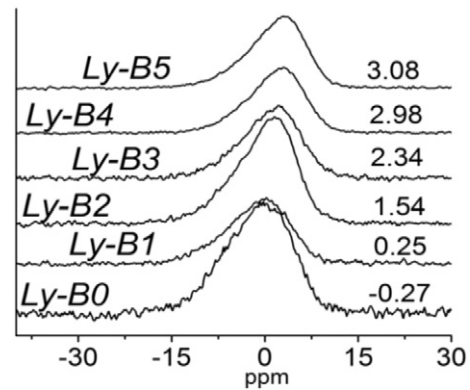

Fig. 5. ^{31}P MAS-NMR spectra of the borate-based glass series. The peak position of each glass is tagged on the right side.

network modifier [11,18]. It has been reported that T_g decreases with the formation of NBOs which is induced by an increased concentrations of network modifiers, because NBOs can cause de-polymerization of the glass network [11]. However, as shown in Fig. 4, T_g gradually increases with increased Sr^{2+} contents in the glass series. It has been reported that there is a positive correlation between T_g and the hardness and the elastic modulus of glasses [34,35].

3.3. ^{31}P and ^{11}B MAS-NMR spectroscopy

The results of MAS-NMR spectroscopy for both ^{31}P and ^{11}B are shown in Figs. 5 and 6, respectively. Considering the chemical composition of the glasses, chemical shifts in the range of −8 to −0.2 ppm [36,37], were recorded in spectra source from ^{31}P MAS-NMR, representing the phosphate tetrahedral structure, where one phosphate atom bonds to two NBOs and one boron atom through an oxygen atom in phosphate-boron glasses. In these glasses, both phosphate and boron act as network formers [36]. Chemical shifts at 5.3 ± 0.2 ppm are assigned to phosphate tetrahedra with three NBOs [38], related to the deconstruction of the phosphorus network [36]. In this borate based glass series, the shifts increased from −0.27 ppm to 3.08 ppm with addition of Sr^{2+} (Fig. 5). The shift to higher ppm values has been confirmed to be related to the depolymerization of the phosphate network [39]. Therefore, it can be concluded that phosphate assumes the role of a network former and the increasing Sr^{2+} contents introduces a higher concentration of NBOs in this glass network.

Two peaks are present in all ^{11}B MAS-NMR spectra. One is a centrally symmetric peak in the region of 0.2 to 0.6 ppm, which is assigned to the four-coordinated borate units (BO_4) [36,37]. The other one is a quadrapole broadened peak, centered at around 11 ppm, which arises
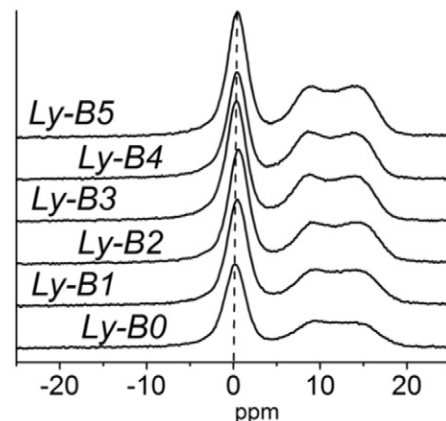

Fig. 4. Glass transition temperature (T_g) of the borate-based glass series.

Fig. 6. ^{11}B MAS-NMR spectra of the borate-based glass series.

Fig. 7. Raman spectra of the borate-based glass series.

network formers, the network modifiers account for 43–63 mol% in the compositions of *Ly-B1* to *Ly-B5*. Thus, more NBOs should be introduced by more addition of Sr^{2+} in the glass series. Therefore, our results of ^{11}B NMR are in good agreement with the previous studies.

3.4. Raman spectroscopy

The resultant Raman spectra are presented in Fig. 7. It is apparent that the spectra are dominated by a broad peak centered at 1320 cm^{-1} with a shoulder at 1500 cm^{-1}. In addition, three Raman bands are exhibited at 770 cm^{-1}, 860 cm^{-1} and 940 cm^{-1}. The intensity of the band at 770 cm^{-1} decreases with increasing Sr^{2+} contents, while the band intensities at 860 cm^{-1} and 940 cm^{-1} increase with addition of Sr^{2+} (observed in the fitted Raman spectra, Fig. 8). Finally, based on the fitted Raman spectra, the peak areas under 860 cm^{-1}, 1320 cm^{-1} and 1500 cm^{-1} increase with increased Sr^{2+} content.

According to previous Raman studies, the peak at 774 cm^{-1} is assigned to the symmetric breathing vibration of six-member rings with one $[BØ_3]$ replaced by $[BØ_4]$ [11,44]. The Raman band at 860 cm^{-1} is related to the symmetric stretching vibrations of B—Ø—B bonds from $[B_2ØO_4]^{4-}$ [44]. Correspondingly, the bands ranging from 1315 to 1350 cm^{-1} are attributed to the stretching vibration of terminal B—O^- bonds of $[B_2ØO_4]^{4-}$ [45]. Raman band at 940 cm^{-1} corresponds to $[BØ_4]$ bonding to NBO-containing groups instead of pure $[BØ_4]$ [46]. The Raman bands centering at 1480–1500 cm^{-1} are due to the presence of $[BO_2O]^-$ [11,45]. The assignments of Raman bands of the borate based glass series are summarized in Table 3.

Therefore, the increasing intensity of Raman bands at 860 cm^{-1}, 940 cm^{-1}, 1320 cm^{-1} and 1500 cm^{-1} indicate the increased presence of $[BØ_2O]^-$ and $[B_2ØO_4]^{4-}$ within the glasses with Sr^{2+} incorporation. It is the formation of NBO that make $[BØ_3]$ and $[BØ_4]$ units convert into $[BØ_2O]^-$ and $[B_2ØO_4]^{4-}$ [11]. The results of Raman spectroscopy demonstrate that the increased addition of Sr^{2+} induces more NBOs in the glass network, which confirm the results of MAS-NMR spectroscopy.

The results of MAS-NMR and Raman spectroscopy indicate that increasing Sr^{2+} content within this glass series introduces more NBOs in the glass structure. Therefore, T_gs of the glasses will be expected to decrease with increased addition of Sr^{2+}. However, this is inconsistent with the results of DTA. It is postulated that boron-oxygen bonding, or the ratio of NBO/BO, is not the only factor influencing T_g. A second factor is metal-oxygen bonding (R—O) which provides additional cross links across the borate segments of the glass network which influences T_g

from the presence of trigonal boron units (BO_3) [34,36]. Based on previous studies of ^{11}B MAS-NMR, BO_4 units and BO_3 units are assigned in the region of −10 to 2 ppm [34,37] and 5 to 15 ppm [36], respectively. The BO_3 quadrupolar line can be approximated as a Gaussian in order to obtain the relative ratio of BO_3 and BO_4 units [38]. The ratio of N_4 (BO_4 / ($BO_3 + BO_4$)) in the six glasses (from *Ly-B0* to *Ly-B5*) are: 0.47, 0.43, 0.42, 0.41, 0.40 and 0.37. This fact indicates that more NBOs were introduced in the glass network with more addition of Sr^{2+} contents in the glass series. Previous studies [40,41] of borate glasses have suggested that the fraction of N_4 in the glass decreased with increasing addition of glass network modifiers, particularly when they account for >40 mol% [42,43], of the glass compositions. It has been reported that boroxol ($BØ_3$) and tetraborate ($BØ_4$) groups are predominant in borate glasses when they contain <20 mol% of network modifiers. The tetraborate ($BØ_4$) and diborate group ($B_4O_5Ø_4^-$) (O = NBO) become the prevalent groups in borate glasses when 20–30 mol% network modifiers are incorporated [13]. Borate glasses with 35–50 mol% of network modifiers consist of diborate units, ring-type metaborate units (metaborate $BØ_2O^-$), pyroborate units ($B_2ØO_4^{4-}$) and orthoborate units (BO_3^{3-}). In this project, since only B_2O_3 and P_2O_5 are the glass
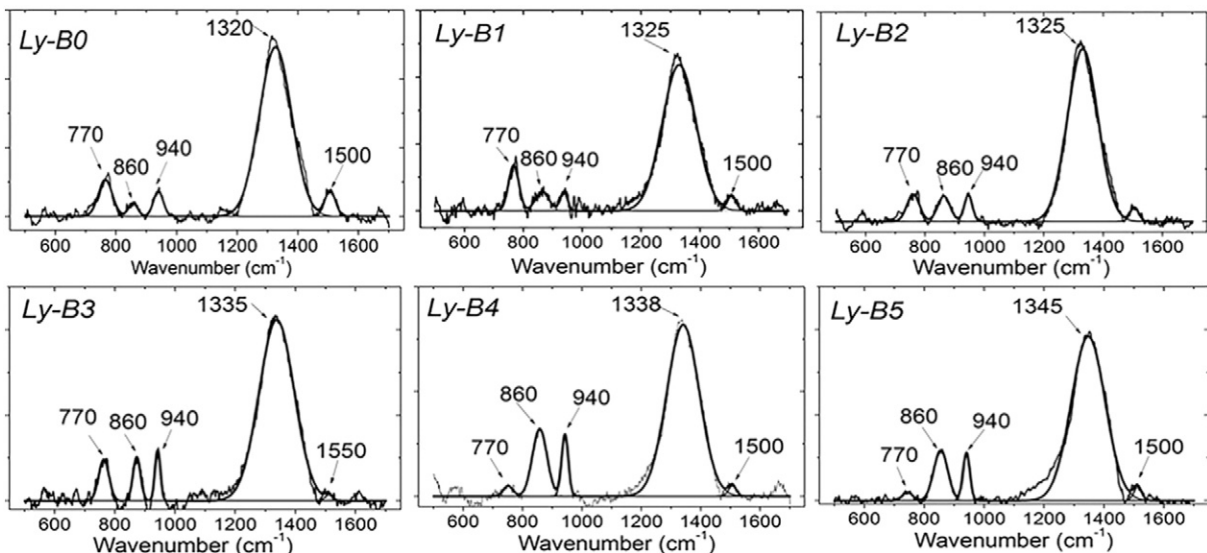

Fig. 8. Fitted Raman spectra of the borate-based glass series.

Table 3
Assignments of Raman bands of the borate-based glass series.

Wavelength (cm^{-1})	Assignments
~770	A structure with two [BØ$_4$] [44].
~860	Symmetric stretching vibrations of B—Ø—B bonds from [B$_2$ØO$_4$]$^{4-}$ [44].
~935–955	Large superstructure group with one (B$_2$O$_6$Ø$_4^-$ pentaborate group) or two (B$_4$O$_5$Ø$_4^-$ diborate group) [BØ$_4$] tetrahedra [46].
~1315–1350	The stretching vibration of terminal B—O$^-$ bonds of [B$_2$ØO$_4$]$^{4-}$ [39,40].
~1480–1500	The structure of [BO$_2$O] [11,45].

[11]. The ionic R—O bonding increases T$_g$ by enhancing network rigidity; the effect depending on the strength of R—O (F$_{R-O}$), which was defined as [11]:

$$F_{R-O} = 4\pi^2 C^2 \mu v_{eff}^2 \qquad (2)$$

where C = speed of light, μ = reduced mass of cation site vibration, and v_{eff} = effective cation site vibration frequency in FT-IR analysis [11].

The literature confirms that T$_g$s of borate glasses increase with the enhancement of F$_{R-O}$ [47]. In addition, F$_{R-O}$s of alkaline earth ions, such as Ca^{2+} and Sr^{2+}, are higher than those of alkali ions, such as Na$^+$ and K$^+$, because divalent ions provide higher coordination numbers with oxygen atoms [48]. Other studies [49,50] have demonstrated that increasing Sr^{2+} content gradually increases T$_g$ in borate-based glass systems. As a result, the increasing amount of Sr—O bonding in the glass structure lead to a gradual increase in T$_g$.

3.5. Measured critical strain energy release rate (G$_{IC}$) of the constructs

The G$_{IC}$ values and the thickness of the glass coatings are shown in Fig. 9. The mean thickness of the coatings was approximately 95 μm, and there was no significant difference ($p \geq 0.05$) among the thicknesses of all the samples. The mean G$_{IC}$ values increased from 6.56 J/m^2 for the system using the Ly-B0 glass to 14.61 J/m^2 for the Ly-B5. The increase in G$_{IC}$ with 15–25 mol% addition of Sr^{2+} contents in the glass series, i.e., Ly-B3, Ly-B4 and Ly-B5, was statistically significant ($p \leq 0.05$), while there was no significant difference ($p \geq 0.05$) among the G$_{IC}$ values for Ly-B0, Ly-B1 and Ly-B2. A previous study of borate glasses found that a higher Young's modulus generally correlated with a higher fracture toughness [51]. In addition, T$_g$ has been proven to correlate positively with Young's modulus [34,35]. In the present study, T$_g$ increased with Sr^{2+} addition in the glass compositions. Thus, we assumed that the observed increases

in G$_{IC}$ with increasing Sr^{2+} contents could be linked to the associated increase in T$_g$.

There is limited literature around G$_{IC}$ data for bioactive glass, bioceramic and glass ceramic coatings. Previous studies have reported G$_{IC}$ values of 0.8 J/m^2 for a bioceramic coating on an aluminum substrate [52], and 0.065 J/m^2 for a glass-ceramic trabecular-like coating on a ceramic substrate [53]. Another study indicated that G$_{IC}$ of a silicate glass coating with thickness of 90 μm was 6.2 J/m^2 [28]. Since G$_{IC}$ can be a measurement of the fracture toughness of the coating/substrate system [54], we concluded that the incorporation of 15–25 mol% Sr^{2+} enhanced the fracture toughness of the glass coating/Ti6Al4V substrate system.

4. Conclusions

In this borate-based glass series, increasing Sr^{2+} content induced the formation of larger amounts of NBOs. The high strength of ionic Sr—O bonding, which provides additional cross links across borate segments of the glass network, had a greater impact than NBO formation on the variation of T$_g$s, leading to gradual increases of T$_g$s with Sr^{2+} addition. The mean G$_{IC}$ values of the coating/substrate system were 6.56–14.61 J/m^2 from Ly-B0 to Ly-B5. The incorporation of 15–25 mol% Sr^{2+} significantly increased the fracture toughness of the borate-based glass coating/Ti6Al4V substrate system.

References

[1] K. Kolan, Borate bioactive glass scaffolds made by the selective laser sintering process, Proceedings of the 8th Annual ISC Graduate Research Symposium, 2014 Rolla, Missouri.
[2] X. Liu, H. Pan, H. Fu, Q. Fu, M.N. Rahaman, W. Huang, Conversion of borate-based glass scaffold to hydroxyapatite in a dilute phosphate solution, Biomed. Mater. 5 (1) (2010) 015005.
[3] N.W. Marion, W. Liang, G.C. Reilly, D.E. Day, M.N. Rahaman, J.J. Mao, Borate glass supports the in vitro osteogenic differentiation of human mesenchymal stem cells, Mech. Adv. Mater. Struct. 12 (3) (2005) 239–246.
[4] A. Yao, D. Wang, W. Huang, Q. Fu, M.N. Rahaman, D.E. Day, In vitro bioactive characteristics of borate-based glasses with controllable degradation behavior, J. Am. Ceram. Soc. 90 (1) (2007) 303–306.
[5] J. Ning, A. Yao, D. Wang, W. Huang, H. Fu, X. Liu, X. Jiang, X. Zhang, Synthesis and in vitro bioactivity of a borate-based bioglass, Mater. Lett. 61 (30) (2007) 5223–5226.
[6] A. Yao, D. Wang, Q. Fu, W. Huang, M.N. Rahaman, Preparation of bioactive glasses with controllable degradation behavior and their bioactive characterization, Chin. Sci. Bull. 52 (2) (2007) 272–276.
[7] R.F. Brown, M.N. Rahaman, A.B. Dwilewicz, W. Huang, D.E. Day, Y. Li, B.S. Bal, Effect of borate glass composition on its conversion to hydroxyapatite and on the proliferation of MC3T3-E1 cells, J. Biomed. Mater. Res. A 88 (2) (2009) 392–400.
[8] L. Bi, B. Zobell, X. Liu, M.N. Rahaman, L.F. Bonewald, Healing of critical-size segmental defects in rat femora using strong porous bioactive glass scaffolds, Mater. Sci. Eng. C 42 (2014) 816–824.
[9] Z. Xie, X. Liu, W. Jia, C. Zhang, W. Huang, J. Wang, Treatment of osteomyelitis and repair of bone defect by degradable bioactive borate glass releasing vancomycin, J. Control. Release 139 (2) (2009) 118–126.
[10] W.-T. Jia, X. Zhang, S.-H. Luo, X. Liu, W.-H. Huang, M.N. Rahaman, D.E. Day, C.-Q. Zhang, Z.-P. Xie, J.-Q. Wang, Novel borate glass/chitosan composite as a delivery vehicle for teicoplanin in the treatment of chronic osteomyelitis, Acta Biomater. 6 (3) (2010) 812–819.
[11] Y. Yiannopoulos, G.D. Chryssikos, E. Kamitsos, Structure and properties of alkaline earth borate glasses, Phys. Chem. Glasses 42 (3) (2001) 164–172.
[12] D. Grseom, Borate Glasses Structure, Properties and Applications, Plenum Press, New York, 1978.
[13] W.L. Konijnendijk, J.M. Stevels, The structure of borate glasses studied by Raman scattering, J. Non-Cryst. Solids 18 (3) (1975) 307–331.
[14] L. Peddi, R.K. Brow, R.F. Brown, Bioactive borate glass coatings for titanium alloys, J. Mater. Sci. Mater. Med. 19 (9) (2008) 3145–3152.
[15] W. Xiao, S.-H. Luo, X.-J. Wei, C.-Q. Zhang, W.-H. Huang, J.-K. Chen, Y. Cai, Y. Rui, M.N. Rahaman, Evaluation of Ti implants coated with Ag-containing borate bioactive glass for simultaneous eradication of infection and fracture fixation in a rabbit tibial model, J. Mater. Res. 27 (24) (2012) 3147–3156.
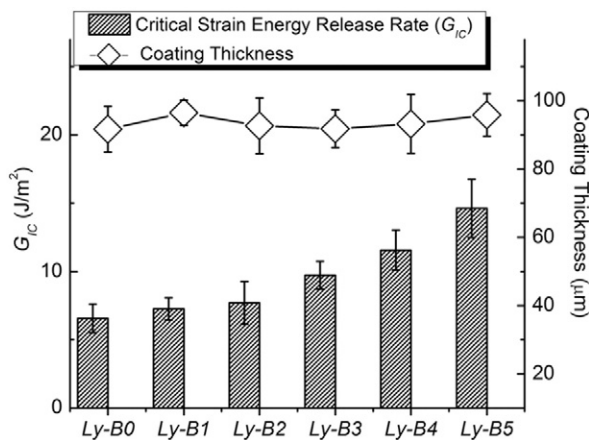

Fig. 9. The critical strain energy release rate (G$_{IC}$) and the thickness of the borate-based glass coatings-Ti6Al4V substrate system. Scatter bars indicate the standard deviation of the data.

[16] D. Bellucci, V. Cannillo, A. Sola, Coefficient of thermal expansion of bioactive glasses: available literature data and analytical equation estimates, Ceram. Int. 37 (8) (2011) 2963–2972.

[17] Y.-P. Lu, M.-S. Li, S.-T. Li, Z.-G. Wang, R.-F. Zhu, Plasma-sprayed hydroxyapatite titania composite bond coat for hydroxyapatite coating on titanium substrate, Biomaterials 25 (18) (2004) 4393–4403.

[18] Y. Li, A. Coughlan, F. Laffir, D. Pradhan, N. Mellott, A. Wren, Investigating the mechanical durability of bioactive glasses as a function of structure, solubility and incubation time, J. Non-Cryst. Solids 380 (2013) 25–34.

[19] M. O'Donnell, P. Candarlioglu, C. Miller, E. Gentleman, M. Stevens, Materials characterisation and cytotoxic assessment of strontium-substituted bioactive glasses for bone regeneration, J. Mater. Chem. 20 (40) (2010) 8934–8941.

[20] S. Dahl, P. Allain, P. Marie, Y. Mauras, G. Boivin, P. Ammann, Y. Tsouderos, P. Delmas, C. Christiansen, Incorporation and distribution of strontium in bone, Bone 28 (4) (2001) 446–453.

[21] I.D. Learmonth, C. Young, C. Rorabeck, The operation of the century: total hip replacement, Lancet 370 (9597) (2007) 1508–1519.

[22] S.A. Goldstein, The mechanical properties of trabecular bone: dependence on anatomic location and function, J. Biomech. 20 (11) (1987) 1055–1061.

[23] E. Mohseni, E. Zalnezhad, A. Bushroa, Comparative investigation on the adhesion of hydroxyapatite coating on Ti–6Al–4V implant: a review paper, Int. J. Adhes. Adhes. 48 (2014) 238–257.

[24] Y.-C. Yang, E. Chang, S. Lee, Mechanical properties and Young's modulus of plasma-sprayed hydroxyapatite coating on Ti substrate in simulated body fluid, J. Biomed. Mater. Res. A 67 (3) (2003) 886–899.

[25] A. Sola, D. Bellucci, V. Cannillo, Enamelled coatings produced with low-alkaline bioactive glasses, Surf. Coat. Technol. 248 (2014) 1–8.

[26] R. Geesink, K. de Groot, C. Klein, Bonding of bone to apatite-coated implants, J. Bone Joint Surg. (Br.) 70 (1) (1988) 17–22.

[27] A. Lynn, D. DuQuesnay, Hydroxyapatite-coated Ti–6Al–4V: part 1: the effect of coating thickness on mechanical fatigue behaviour, Biomaterials 23 (9) (2002) 1937–1946.

[28] A. Matinmanesh, O. Rodriguez, M. Towler, P. Zalzal, E. Schemitsch, M. Papini, Quantitative evaluation of the adhesion of bioactive glasses onto Ti6Al4V substrates, Mater. Des. 97 (2016) 213–221.

[29] S. Zhang, Z. Xianting, W. Yongsheng, C. Kui, W. Wenjian, Adhesion strength of sol–gel derived fluoridated hydroxyapatite coatings, Surf. Coat. Technol. 200 (22) (2006) 6350–6354.

[30] B.R. Lawn, A. Evans, D. Marshall, Elastic/plastic indentation damage in ceramics: the median/radial crack system, J. Am. Ceram. Soc. 63 (9–10) (1980) 574–581.

[31] A.K. Bhattacharya, J.J. Petrovic, S.C. Danforth, Indentation method for determining the macroscopic fracture energy of brittle bimaterial interfaces, J. Am. Ceram. Soc. 75 (2) (1992) 413–417.

[32] A. Ameli, M. Papini, J. Spelt, Evolution of crack path and fracture surface with degradation in rubber-toughened epoxy adhesive joints: application to open-faced specimens, Int. J. Adhes. Adhes. 31 (6) (2011) 530–540.

[33] Y. Li, L. Placek, A. Coughlan, F. Laffir, D. Pradhan, N. Mellott, A. Wren, Investigating the influence of Na^+ and Sr^{2+} on the structure and solubility of SiO_2–TiO_2–CaO–Na_2O/SrO bioactive glass, J. Mater. Sci. Mater. Med. 26 (2) (2015) 1–12.

[34] W. Wang, Elastic moduli and behaviors of metallic glasses, J. Non-Cryst. Solids 351 (16) (2005) 1481–1485.

[35] T. Watanabe, K. Muratsubaki, Y. Benino, H. Saitoh, T. Komatsu, Hardness and elastic properties of Bi_2O_3-based glasses, J. Mater. Sci. 36 (10) (2001) 2427–2433.

[36] R. Christensen, G. Olson, S.W. Martin, Structural studies of mixed glass former 0.35 Na_2O + 0.65 [x B_2O_3 + (1 − x) P_2O_5] glasses by Raman and [11]B and ^{31}P magic angle spinning nuclear magnetic resonance spectroscopies, J. Phys. Chem. B 117 (7) (2013) 2169–2179.

[37] M. Zeyer-Düsterer, L. Montagne, G. Palavit, C. Jäger, Combined ^{17}O NMR and ^{11}B–^{31}P double resonance NMR studies of sodium borophosphate glasses, Solid State Nucl. Mag. 27 (1) (2005) 50–64.

[38] D. Qiu, P. Guerry, I. Ahmed, D.M. Pickup, D. Carta, J.C. Knowles, M.E. Smith, R.J. Newport, A high-energy X-ray diffraction, ^{31}P and ^{11}B solid-state NMR study of the structure of aged sodium borophosphate glasses, Mater. Chem. Phys. 111 (2) (2008) 455–462.

[39] R.K. Brow, Review: the structure of simple phosphate glasses, J. Non-Cryst. Solids 263 (2000) 1–28.

[40] P.J. Bray, NMR studies of the structures of glasses, J. Non-Cryst. Solids 95 (1987) 45–59.

[41] Y. Yun, P.J. Bray, B11 nuclear magnetic resonance studies of Li2O B2O3 glasses of high Li2O content, J. Non-Cryst. Solids 44 (2–3) (1981) 227–237.

[42] P. Bray, S. Feller, G. Jellison, Y. Yun, B 10 NMR studies of the structure of borate glasses, J. Non-Cryst. Solids 38 (1980) 93–98.

[43] Y. Yun, P. Bray, Nuclear magnetic resonance studies of the glasses in the system Na2O B2O3 SiO2, J. Non-Cryst. Solids 27 (3) (1978) 363–380.

[44] E. Anghel, M. Zaharescu, S. Zuca, E. Pavlatou, Structure and phase diagram of the $Na_2B_4O_7$–Na_3AlF_6 system, J. Mater. Sci. 34 (16) (1999) 3923–3929.

[45] E. Kamitsos, M. Karakassides, G.D. Chryssikos, Vibrational spectra of magnesium-sodium-borate glasses. 2. Raman and mid-infrared investigation of the network structure, J. Phys. Chem. 91 (5) (1987) 1073–1079.

[46] A.A. Osipov, L.M. Osipova, Raman scattering study of barium borate glasses and melts, J. Phys. Chem. Solids 74 (7) (2013) 971–978.

[47] Y. Yiannopoulos, G.D. Chryssikos, E. Kamitsos, Structure and properties of alkaline earth borate glasses, Phys. Chem. Glasses-B 42 (3) (2001) 164–172.

[48] J. Lao, J.-M. Nedelec, E. Jallot, New strontium-based bioactive glasses: physicochemical reactivity and delivering capability of biologically active dissolution products, J. Mater. Chem. 19 (19) (2009) 2940–2949.

[49] H. Sinouh, L. Bih, M. Azrour, A. El Bouari, S. Benmokhtar, B. Manoun, B. Belhorma, T. Baudin, P. Berthet, D. Solas, Effect of TiO_2 and SrO additions on some physical properties of $33Na_2O$–$xSrO$–$xTiO_2$–$(50 − 2x)$ B_2O_3–$17P_2O_5$ glasses, J. Therm. Anal. Calorim. 111 (1) (2013) 401–408.

[50] Y. Ohta, M. Shimada, M. Koizumi, Properties and structure of lithium borate and strontium borate glasses, J. Am. Ceram. Soc. 65 (11) (1982) 572–574.

[51] N. Shinkai, R. Bradt, G.E. Rindone, Elastic modulus and fracture toughness of ternary PbO-ZnO-B_2O_3 glasses, J. Am. Ceram. Soc. 65 (2) (1982) 123–126.

[52] F. Baino, C. Vitale-Brovarone, Wollastonite-containing bioceramic coatings on alumina substrates: design considerations and mechanical modelling, Ceram. Int. 41 (9) (2015) 11464–11470.

[53] Q. Chen, F. Baino, N.M. Pugno, C. Vitale-Brovarone, Bonding strength of glass-ceramic trabecular-like coatings to ceramic substrates for prosthetic applications, Mater. Sci. Eng. C 33 (3) (2013) 1530–1538.

[54] T.L. Anderson, T. Anderson, Fracture Mechanics: Fundamentals and Applications, CRC Press, 2005.